`Journal of the Nigerian Association of Mathematical Physics
Volume 59 **(January – March *2021 Issue*), pp53 – 60**

VIBRATIONAL RESONANCE IN AN OSCILLATOR MODELLED BY DIHEDRAL POTENTIAL

O. I. Olusola[1], E. O. Ogungbemi[1], K. S. Oyeleke[1] and U. E. Vincent[2,3]

[1]Department of Physics, University of Lagos, Lagos, Nigeria.
[2]Department of Physical Sciences, Redeemer's University, P.M.B. 230, Ede, Nigeria.
[3]Department of Physics, Lancaster University, Lancaster LA1 4YB, United Kingdom.

Abstract

This paper examines and analyses the vibrations of a particle situated in a dihedral potential and subjected to dual frequency forcing. Based on the method of separation of time scales, the response amplitude of the particle at low-frequency (LF) is theoretically derived. It is found that a close agreement exists between the theoretical prediction and numerical simulation. The presence of externally applied electric field could be optimized to promote large amplitude multiple vibrational resonances.

Keywords: Oscillations, Vibrations, Resonance, dihedral potential

1. Introduction

For many years, noise was widely understood to constitute a nuisance in a system, mainly due to its capabilities to distort signal processing. However, in 1981 a remarkable turning point occurred when Benzi et al. [1] demonstrated the positive influence of noise in enhancing weak signal. This breakthrough popularly known as stochastic resonance (SR) reported in Ref. [1] has attracted the attention of many researchers and has remained a subject of intense research focus in recent time [2–8]. About two decades later, it was demonstrated numerically by Landa and McClintock [9] that when the noisy input in SR framework is replaced with appropriate high frequency (HF) harmonic force field, a related phenomenon termed vibrational resonance (VR) occurred [9]; and was later analysed theoretically [10]. Following these pioneering works, the phenomenon of VR has been experimentally demonstrated in physical systems such as bistable and multistable vertical-cavity surface-emitting lasers (VCSELs) [11–13].

Some studies on VR have shown that enhancement in the system's response takes place at the bifurcation of effective potential of slow motion of the system. For this purpose, research attentions have been focused on the possible roles played by the system's bifurcation parameters [14–16], nonlinear dissipation [17–19], fractional order [20–22], and delay [23–25] on the generation and suppression of VR. Recently [26], it was also shown that system's parameters can be modified to control the depth and location of wells in the system's potential as a means of enhancing VR in quintic oscillators. Very recently, research efforts have proven that VR can be induced in time-delayed fractional order quintic oscillator system when the fractional order term is varied, and the bifurcation point changes periodically as the time delay is varied progressively [22]. In some very recent reports, we have proved the existence of response amplification induced by deformation in an asymmetric deformed potential [27] as well as the possibility of roughness-induced resonances in a rough potential [28]. In the quantum domain, VR is also being explored in quantum mechanical oscillators, such as the Tietz Hua potential well, in which quantum VR was demonstrated theoretically and numerically [29].

Despite the huge body of knowledge outlined in the previous works, we note that non has been devoted to systems modelled by united atom model - a class of systems consisting of bounded and unbounded potentials [30–32]. One of the bounded potentials describing the united atom model is the dihedral potential which has been studied extensively [32,33]. For example, in complex medium such as polymers, the potential has been explored on a molecular level to examine polymer crystallisation under quiescent conditions as well as large deformations [32, 34–38]. In addition, the potential find numerous applications in organic electronics for organic light emitting diodes, organic solar cells as well as in organic and inorganic substances at atomic levels and other scientific and engineering applications [See Ref. [39] and the references therein]. Recently, Nicholson and Rutledge [33], employed dihedral potential to examine flow induced crystallization of linear polymer chains comprising 1000 polymers. The dihedral potential has been studied and shown to be useful from

Corresponding Author**:** Olusola O.I., Email: iolusola@unilag.edu.ng, Tel: +2348034778641

scientific and technologic point of views. In particular, in the polymer processing, its understanding is vital for industrial production of materials with desired mechanical, optical and thermal properties.

Thus, we investigate nonlinear response in the framework of vibrational resonance when a particle moving the dihedral potential is subjected to dual frequency driving forces. Moreover, we derived analytical expression of response amplitude for the values of systems inherent parameters at which VR occurs. Our analytical result is validated with numerical experiments, showing that both are consistent. The paper also reports the occurrence of multiple resonance peaks with variation in the fast motion parameters.

The rest of this paper is structured as follows: In section 2, the proposed model is presented. Section 3 is focused on the theoretical analyses for the occurrence of VR. In section 4 the results obtained from the numerical experiments are discussed. The paper is summarized and conclusions drawn in section 5.

2. The Model and its dynamics

In this paper, we examined VR in an oscillator modelled by dihedral potential [33]. The equation of motion for a particle biharmonically driven by two widely varying frequencies ($\omega \ll \Omega$) in the potential may be written as follows:

$$\ddot{\phi} + b\dot{\phi} + \frac{du(\phi)}{d\phi} = f\,cos(\omega t) + g\,cos(\Omega t), \quad (1)$$

where b is the damping coefficient, $\mathcal{U}(\phi)$ is the dihedral potential, $fcos(\omega t)$ and $gcos(\Omega t)$ are respectively low-input signal and high-input signal with frequency $\omega \ll \Omega$. The potential of system (1) is given by:

$$\mathcal{U}(\phi) = \frac{1}{2}[\gamma_1(1 - cos\,\phi) + \gamma_2(1 - cos\,2\,\phi) + \gamma_3(1 - cos\,3\,\phi)], \quad (2)$$

where γ_i(i = 1, 2, 3) are the dihedral specific force field parameters. The potential, $\mathcal{U}(\phi)$ against ϕ is shown in Figure 1. The following parameters were chosen: $b = 0.5$ γ_1 = 1.6, γ_2 = −0.867, γ_3 = 3.24; and ω = 2. The equilibrium point of the unforced system has three minima located at (0, ±2) around which oscillatory motion of the driven particle takes place.

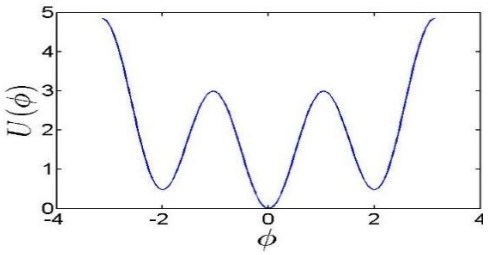

Fig. 1 (Colour online) The potential of system (1) against ϕ with the following parameters: $b = 0.5$, γ_1 = 1.6, γ_2 = −0.867, γ_3 = 3.24; and ω = 2

The shape of potential depends only on three parameters (γ_1, γ_2, and γ_3) which is different from quintic oscillator in which the shape of the potential depends on four parameters(${\omega^2}_0, \beta, \xi,\ and\ \gamma$) [22].

In order to examine the stability of fixed points of the system in the absence of external forcing, equation (1) can be expressed as two coupled autonomous ordinary differential equations (ODEs) in the form:

$$\frac{d\phi_1}{dt} = \phi_2 \quad (3)$$

$$\frac{d\phi_2}{dt} = -b\phi_2 - \frac{1}{2}\left(\gamma_1 \sin\phi_1 + 2\gamma_2 \sin 2\phi_1 + 3\gamma_3 \sin 3\phi_1\right).$$

The equilibrium points of system (3) are found by solving the following system of equations with parameters taken as $b = 0.5, \gamma_1$ = 1.6, γ_2 = −0.867, γ_3 = 3.24:

$$\phi_2 = 0$$

$$-b\phi_2 - \frac{1}{2}\left(\gamma_1 \sin\phi_1 + 2\gamma_2 \sin 2\phi_1 + 3\gamma_3 \sin 3\phi_1\right) = 0. \quad (4)$$

By linearizing the system, it yields the Jacobian matrix:

$$J(\phi) = \begin{vmatrix} 0 & 1 \\ K & -b \end{vmatrix}, \quad (5)$$

where $K = -\frac{1}{2}(\gamma_1 \cos\phi_1 + 4\gamma_2 \cos 2\phi_1 + 9\gamma_3 \cos 3\phi_1)$. The characteristics equation is given as

$$\lambda^2 - b\lambda + K = 0 \quad .$$

$$\lambda_{1,2} = \frac{b \pm \sqrt{b^2 - 4K}}{2}$$

Considering equilibrium point $E_a(0,0)$; the eigenvalues of $J(E_a)$ are computed as $\lambda_{1,2} = -0.2500 \pm 3.6856i$. Thus E_a is a stable focus. Also, for equilibrium point $E_b(-2,2)$, the eigenvalues are computed as $\lambda_{1,2} = -0.2500 \pm 3.8389i$. Thus E_b is also a stable focus. For equilibrium point $E_c(-1,1)$, the eigenvalues are computed as $\lambda_1 = -3.9028$ and $\lambda_2 = 3.4028$. Thus, E_c is a saddle and therefore unstable. $E_a(0,0)$, $E_b(-2,2)$ and $E_c(-1,1)$ re-affirm the equilibrium positions in Figure 1.

3. Theoretical Analysis

In the following, VR would be analysed in system (1) ($f \ll g$ *and* $\omega \ll \Omega$.) expressed in the form:

$$\ddot{\phi} = -b\dot{\phi} - \frac{1}{2}(\gamma_1 \sin\phi + 2\gamma_2 \sin 2\phi + 3\gamma_3 \sin 3\phi) + f\cos(\omega t) + g\cos(\Omega t). \quad (6)$$

Our aim is to derive and compute the response amplitude, Q_{anal} as a function of the system's parameter. Due to the action of the biharmonic force fields, $f\cos(\omega t)$ and $g\cos(\Omega t)$ with $\omega \ll \Omega$, the motion of Eq. (3) consists of a slow motion and a fast motion. In this regard, the method of direct separation of motions described by Blekhman [40] and frequently used by many authors is employed for the analysis. This gives us a set of integro-differential equations consisting of slow motion of the system whose response can be modulated by adjusting the parameters of the high-frequency force field. Based on this method, the solution of Equation (3) is assumed to be comprised of a slow motion $\chi(t)$ with period T = $\frac{2\pi}{\omega}$ and a fast motion $\psi(t, \Omega t)$ with period T = $\frac{2\pi}{\Omega}$ i.e.

$$\phi(t) = \chi + \psi \quad . \quad (7)$$

The mean value of the fast oscillatory signal ψ with respect to fast time $\tau = \Omega t$ is given by:

$$\overline{\psi} = \frac{1}{2\pi}\int_0^{2\pi} \psi \, d\tau = 0 \quad . \quad (8)$$

Substituting equation (7) into equation (6), we have,

$$\ddot{\chi} + \ddot{\psi} + b\dot{\chi} + \lambda\dot{\psi} + \frac{1}{2}(\gamma_1 \sin(\chi + \psi)) + \left(\gamma_2 \sin 2(\chi + \psi)\right) + \frac{3}{2}\left(\gamma_3 \sin 3(\chi + \psi)\right) = f\cos(\omega t) + g\cos(\Omega t). \quad (9)$$

We can express the function $\sin(\chi + \psi)$ using trigonometry identity (i.e. $\sin(\chi + \psi) = \sin\chi\cos\psi + \cos\chi\sin\psi$) and averaging Equation (9) w.r.t. fast motion component to obtain,

$$\ddot{\chi} + b\dot{\chi} + \frac{1}{2}\gamma_1\left(\sin\chi\,\overline{\cos\psi} + \cos\chi\,\overline{\sin\psi}\right) + \gamma_2\left(\sin 2\chi\,\overline{\cos 2\psi} + \cos 2\chi\,\overline{\sin 2\psi}\right) + \frac{3}{2}\gamma_3\left(\sin 3\chi\,\overline{\cos 3\psi} + \cos 3\chi\,\overline{\sin 3\psi}\right) = f\cos(\omega t). \quad (10)$$

Subtracting Equation (10) from Equation (9) yields

$$\ddot{\psi} + b\dot{\psi} + \frac{1}{2}\gamma_1\left(\sin\chi\left(\cos\psi - \overline{\cos\psi}\right) + \cos\chi\left(\sin\psi - \overline{\sin\psi}\right)\right) + \gamma_2\left(\sin 2\chi\left(\cos 2\psi - \overline{\cos 2\psi}\right) + \cos 2\chi\left(\sin 2\psi - \overline{\sin 2\psi}\right)\right) + \frac{3}{2}\gamma_3\left(\sin 3\chi\left(\cos 3\psi - \overline{\cos 3\psi}\right) + \gamma_3\cos\chi\left(\sin 3\psi - \overline{\sin 3\psi}\right)\right) = g\cos(\Omega t). \quad (11)$$

Equations (10) and (11) are the required integro-differential equations of motion for the slow motion χ and the fast motion ψ respectively. Equation (10) is more important for this analysis because it is the equation of motion for the slow dynamics, which is expected to be modulated appropriately by changing the parameters of the fast signal in order to achieve vibrational resonance. Proceeding further, we impose inertia approximation $\ddot{\psi} \gg \dot{\psi} \gg \psi$ on Equation (11) so that $\ddot{\psi} = g\cos(\Omega t)$ with the solution

$$\psi = -\frac{g}{\Omega^2}\cos\Omega t. \quad (12)$$

With ψ in equation (12), we obtain the following mean values

$$\overline{\psi} = 0 \quad , \tag{13}$$

$$\overline{\sin\psi} = \frac{1}{2\pi}\int_0^{2\pi} \sin\psi dt = 0$$

$$\overline{\cos\psi} = \frac{1}{2\pi}\int_0^{2\pi} \cos\psi dt = J_0\left(\frac{g}{\Omega^2}\right)$$

where $J_0\left(\frac{g}{\Omega^2}\right)$ is the zeroth-order Bessel function of the first kind.

Substituting solutions (13) into equation (10) gives

$$\ddot{\chi} + b\dot{\chi} + \frac{\gamma_1}{2}\left(\sin\chi J_0\left(\frac{g}{\Omega}\right)\right) + \gamma_2\left(\sin 2\chi J_0\left(\frac{2g}{\Omega^2}\right)\right) + \frac{3\gamma_3}{2}\left(\sin 3\chi J_0\left(\frac{3g}{\Omega^3}\right)\right) - f\cos(\omega t) = 0 \,. \tag{14}$$

By making the following substitutions

$$C_1 = J_0\left(\frac{g}{\Omega}\right)\frac{\gamma_1}{2} \tag{15}$$

$$C_2 = J_0\left(\frac{2g}{\Omega^2}\right)\gamma_2$$

$$C_3 = 3J_0\left(\frac{3g}{\Omega^3}\right)\frac{\gamma_3}{2}$$

in (14), we obtain

$$\ddot{\chi} + b\dot{\chi} + C_1\sin\chi + C_2\sin 2\chi + C_3\sin 3\chi = f\cos(\omega t)\,. \tag{16}$$

Equation (16) can be treated as the equation of motion of a particle subjected to an external periodic force $f\cos(\omega t)$ and linear damping in the effective potential, $\mathcal{U}_{eff}(\chi)$, given as:

$$U_{eff}(\chi) = -C_1\cos\chi - \frac{C_2\cos 2\chi}{2} - \frac{C_3\cos 3\chi}{3}. \tag{17}$$

Figure 2 shows the plots of $\mathcal{U}_{eff}(\chi)$ against the slow motion component, χ for selected values of the amplitude of the high-frequency signal with fixed parameter values $\gamma_1 = 1.6$, $\gamma_2 = -0.867$, $\gamma_3 = 3.24$; *and* $\omega = 2$. It is evident from Figure 3 that the shape of effective potential depends on the parameters of the modulating signal.

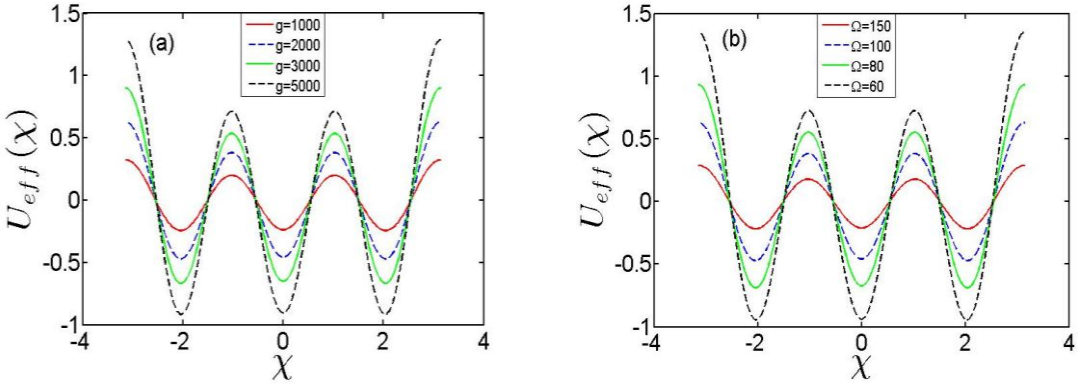

Fig. 2 (Colour online) The shape of effective potential against χ with the following parameters: $b = 0.5$, $\gamma_1 = 1.6$, $\gamma_2 = -0.867$, $\gamma_3 = 3.24$; *and* $\omega = 2$

By considering Equation (17), and Figure 2, the effective potential of the slow motion depends essentially on the parameters (g and Ω) of the fast motion. Therefore, by varying the parameter g (or Ω) of the fast signal, appropriately, one can easily verify the appearance of resonances. It is obvious from Figure 2 that both the height and depth of the effective potential depends on the parameters of the modulating signal. This happens because the parameter (g or Ω) dictates the equilibrium point of the slow dynamics which can be computed from equation (14) as

$$\frac{\gamma_1}{2}\left(\sin\chi J_0\left(\frac{g}{\Omega^2}\right)\right) + \gamma_2\left(\sin 2\chi J_0\left(\frac{2g}{\Omega^2}\right)\right) + \frac{3\gamma_3}{2}\left(\sin\chi J_0\left(\frac{g}{\Omega^2}\right)\right) = 0, \tag{18}$$

thereby yielding a simple stable equilibrium at $\chi^* = 0$

With $J_0 > 0$, the minima of $\mathcal{U}_{eff}(\chi)$ are $\chi^*_{min} = \pm 2n\pi$, n = 0, 1, 2, 3 . . . and the maxima are located at $\chi^*_{max} = \pm(2n + 1)\pi$. The location of the minima and maxim are interchanged when the values of J_0 changes. A slow oscillation occurs about the equilibrium point χ^*. Thus, by perturbing the system about the equilibrium point, $\chi^* = 0$, at which the motion takes place, $\delta = \chi - \chi^*$ is introduced in (14) so that slow oscillation occurs and the motion is described by the following equation:

$$\ddot{\delta} + \ddot{\chi} * + b\dot{\delta} + b\dot{\chi} * + C1\left(sin\,\delta\, cos\,\chi * + cos\,\delta\, sin\ \chi^*\right) + C2\left(sin\,2\,\delta\, cos\,2\ \chi^* + cos\,2\,\delta\, sin\,2\ \chi^*\right) + C3\left(sin\,3\,\delta\, cos\,3\ \chi^* + cos\,3\,\delta\, sin\,3\ \chi^*\right) = f\, cos(\omega t) \quad . \tag{19}$$

By considering a small deviation from the equilibrium point, $\chi^* = 0$, we can take $sin\delta \approx \delta$, $sin2\delta \approx 2\delta$ and $sin3\delta \approx 3\delta$, so that at the equilibrium point we have

$$\ddot{\delta} + b\dot{\delta} + C_1\,\delta + 2C_2\,\delta + 3C_3\delta = f\, cos(\omega t). \tag{20}$$

If $J_0\left(\frac{g}{\Omega^2}\right) > 0$ (< 0). Then $\chi^* = \chi^*_{min}$ (χ^*_{max}). Therefore, $J_0\left(\frac{g}{\Omega^2}\right)\ cos\chi^* = \left|J_0\left(\frac{g}{\Omega^2}\right)\right|$. For $f \ll 1$, we assume that $|\delta| \ll 1$ and $sin\delta \approx \delta$. By neglecting nonlinear terms in Equation (20), we obtain a linearly damped-driven oscillator whose dynamics is written as:

$$\ddot{\delta} + b\dot{\delta} + \omega_r^2\delta = f\, cos(\omega t). \tag{21}$$

where $\omega_r^2 = C_1 + 2C_2 + 3C_3$ is the resonant frequency. In the long time limit, the solution of Eq. (21) is $\delta(t) = A_L\, cos(\omega t + \theta)\ as\ t \to \infty$ A_L is given as

$$A_L = \frac{f}{[(\omega r^2 - \omega^2)^2 + b^2\omega^2]^{1/2}}. \tag{22}$$

and the phase angle, θ is defined as:

$$\theta = tan^{-1}\left[\frac{b\omega}{\omega^2 - \omega r^2}\right]. \tag{23}$$

In general, the response amplitude, Q_{anal} of the system can be expressed as

$$Q_{anal} = \frac{A_L}{f} = \frac{1}{[(\omega r^2 - \omega^2)^2 + b^2\omega^2]^{1/2}}\ . \tag{24}$$

From Equation (24), resonance (i.e. maximum Q_{anal}) can occur when $S = \omega_r^2 - \omega^2$ is minimum (i.e. $\omega_r = \omega$). In the numerical analysis that follows, the analytical computed response amplitude Q_{anal} is compared with the corresponding numerical result obtained by solving Equation (3) directly.

4 Numerical results and discussion

In order to validate the theoretical result for response amplitude, Q_{anal} in Eq. (24), presented in section 3 we performed numerical experiment by applying the fourth-order Runge-Kutta integration routine to integrate Equation (3) with step size $\Delta t = 0.01\,T$ over a simulation time interval $T_s = n\,T$; $T = \frac{2\pi}{\omega}$ representing the period of the oscillation where ω is the low frequency input signal and positive integer *n* stands for number of complete oscillations. We use initial conditions (ϕ_1, ϕ_2) = (0, 0.5), a relaxation time of $20T$ and fixed the parameters of the system as $b = 0.5$, f = 0.1, ω = 2, $\gamma_1 = 1.6$, $\gamma_2 = -0.867$, $\gamma_3 = 3.24$ throughout the computation. The other parameters of the system are chosen within a regime where VR is optimized. We solved Equation (3) numerically and after discarding the transients, the numerically computed amplitude, Q_{num} was calculated from the Fourier spectrum of the output signal $\phi(t)$with Fourier coefficients Q_s and Q_c based on the following expression

$$Q_{num} = \frac{\sqrt{{Q_s}^2 + {Q_c}^2}}{f}, \tag{25}$$

with Q_s and Q_c being respectively defined as

$$Q_s = \frac{2}{nT}\int_0^{nT} \varphi(t)\, sin\,\omega\, t dt$$

$$Q_c = \frac{2}{nT}\int_0^{nT} \varphi(t)\, cos\,\omega\, t dt, \tag{26}$$

and $T = \frac{2\pi}{\omega}$, and n is a positive integer which should be very large to ensure the convergence of the solution. The numerically computed response amplitude, Q_{num} from Eq. (25) are then compared with the analytical ones, Q_{anal} from Eq. (21) and shown in Figure 3. It is clear that the two results are consistent considering that the analytical calculations have been done based on approximations using the method of the separation of motion on two time scale - fast and slow motion - from which fast motion have been averaged out to obtain Equation (21) while the numerical integration of Equation (3) preserves all the time scales of the dynamics of the system. In Figure 3, the continuous lines represent the numerical response curve obtained from Equation (25) while the dash lines denote theoretical/analytical curve derived from Equation (21).

From Figure 3, it is obvious that in each of the sub-plots the number of peaks that appears for each plot is more than two, indicating the occurrence of multi-resonances. In addition, Figure 3 reveals that the response amplitude, Q reaches the peak when the frequency of slow motion is small. This is a confirmation of an important requirement for the manifestation of VR - that is $\omega \ll \Omega$. However, there is a difference between the numerically computed response amplitude and the analytical ones. For example, when ω = 2.5 in Figure 3(d), the numerically computed response amplitude is about twice the analytical one in magnitude.

The frequency response for different values of g or Ω is shown in Figure 4. The value of g or Ω impacts significantly on the frequency response curve. From Figure 4, it is obvious that as the amplitude of fast motion increases, the maximum response amplitude Q_{max} also increases. For instance, with g = 500, the response amplitude is approximately 2.8 while for g = 1750 the response amplitude becomes approximately 6.8. This implies that in practice one can adjust the parameters (g and/or Ω) of the high frequency forcing, appropriately, in order to achieve the desired frequency response or to avoid some frequency range.

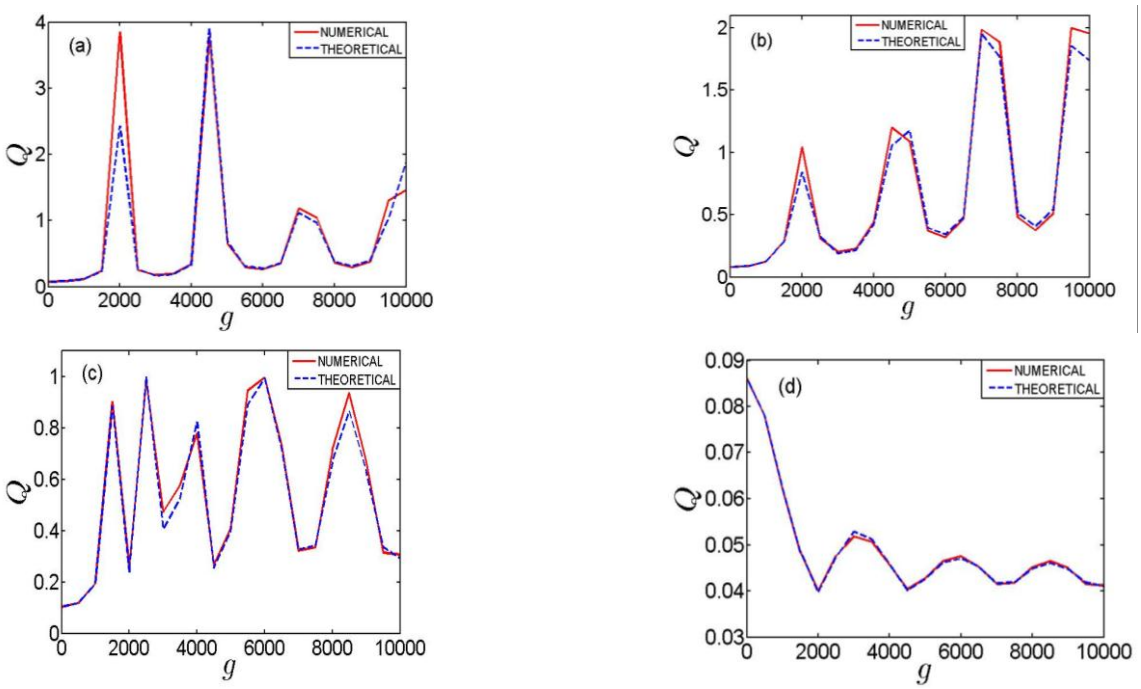

Fig. 3 (Colour online) Evolution of response amplitude, Q, versus amplitude of high signal, g with: (a) ω = 1.0; (b) ω = 1.5; (c) ω = 2.0 and (d) ω = 2.4 and other parameters fixed at b= 0.5, f = 0.1, ω = 2, γ_1 = 1.6, γ_2 = −0.867, γ_3 = 3.24. The continuous lines represent numerically generated Q_{num} from Eq. (23) while the broken lines represent the corresponding analytical values computed from Eq. (21)

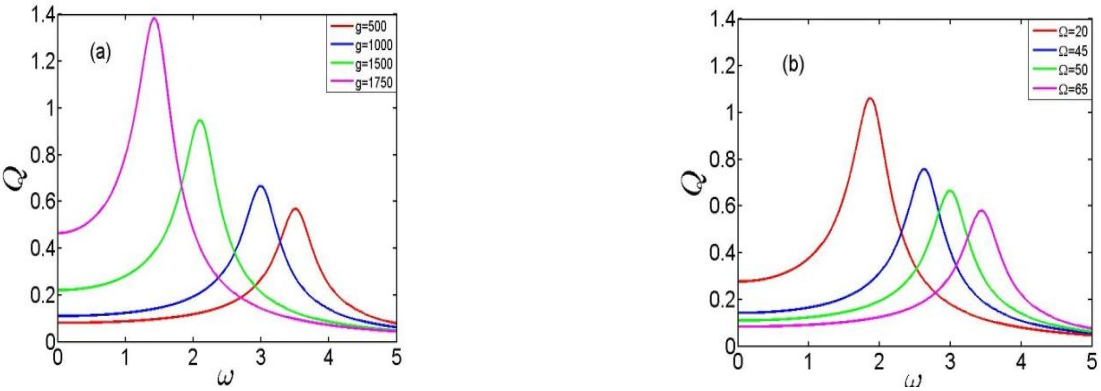

Fig. 4 (Colour online) Frequency response of the system with different values of g and Ω with other parameters fixed at b= 0.5, f = 0.1, ω = 2, γ_1 = 1.6, γ_2 = −0.867, γ_3 = 3.24

5 Conclusion

In this paper, we have examined the response of a particle subjected to bi-harmonic forcing in a dihedral potential. The dihedral potential with triple well is explored based on both analytical and numerical approaches. By applying vibrations mechanics principle in which the slow and fast motions are separated, we predicted the analytical linear response amplitude, indicating the occurrence of VR. It was found that variations in the parameters of the fast signal significantly impact the frequency response of the system and thus lead to the occurrence of multiple VR. Since the approach with low-frequency force field modulated by a high-frequency one has applications in many scientific and technological fields [41-43], we hope that the result presented in this paper would be of importance to these fields. In particular, the presence of high-frequency carrier signal could be of great importance in the tunning the frequency of the power transmission systems in order to eradicate resonance, fundamental frequency should not fall within critical frequency range [44].

References

[1] R. Benzi, A. Sutera, A. Vulpiani, The mechanism of stochastic resonance, *J. Phys. A: Math. Gen.* **14**(11), L453–L457 (1981).

2] S. Fauve, F. Heslot, Stochastic resonance in a bistable system, Phys. Lett. A **97**(1), 5–7 (1983).

[3] B. McNamara, K. Wiesenfeld, R. Roy, Observation of stochastic resonance in a ring laser, *Phys. Rev. Lett.* **60**, 2626–2629 (1988).

[4] L. Gammaitoni, F. Marchesoni, E. Menichella-Saetta, S. Santucci, Stochastic resonance in bistable systems, *Phys. Rev. Lett.* **62**, 349–352 (1989).

[5] M. Gitterman, Harmonic oscillator with multiplicative noise: Nonmonotonic dependence on the strength and the rate of dichotomous noise, *Phys. Rev. E* **67**, 057103, (2003).

[6] M. I. Dykman, D. G. Luchinsky, R. Mannella, P. V. E. McClintock, N. D. Stein, N. G. Stocks, Stochastic resonance in perspective, *Il Nuovo Cimento* D **17**(7) 661–683 (1995).

[7] L. Gammaitoni, P. H¨anggi, P. Jung, F. Marchesoni, Stochastic resonance, *Rev. Modern Phys.* **70**, 223–287 (1998).

[8] P. Sarkar, S. Paul, D. S. Ray, Controlling subharmonic generation by vibrational and stochastic resonance in a bistable system, *J. Stat. Mech.* **2019**(6)**,** 063211 (2019).

[9] P. S. Landa, P. V. E. McClintock, Vibrational resonance, *J. Phys. A: Math. Gen.* **33**(45)**,** L433 (2000).

[10] M. Gitterman, Bistable oscillator driven by two periodic fields, *J. Phys. A: Math. Gen.* **34**(24), L355. 12 (2001).

[11] J. P. Baltan´as, L. L´opez, I. I. Blechman, P. S. Landa, A. Zaikin, J. Kurths, M. A. F. Sanju´an, Experimental evidence, numerics, and theory of vibrational resonance in bistable systems, *Phys. Rev. E* **67**, 066119 (2003).

[12] V. N. Chizhevsky, E. Smeu, G. Giacomelli, Experimental evidence of "vibrational resonance" in an optical system, *Phys. Rev. Lett.* **91**, 220602 (2003).

[13] P. Venkatesh, A. Venkatesan, Vibrational resonance and implementation of dynamic logic gate in a piecewise-linear Murali Lakshmanan Chua circuit, *Commun. Nonlinear Sci.* **39**, 271– 282 (2016).

[14] S. Rajasekar, S. Jeyakumari, V. Chinnathambi, M. A. F. Sanjuan, Role of depth and location of minima of a double-well potential on vibrational resonance, *J. Phys. A: Math. Gen.* **43**(46), 465101 (2010)

[15] J. Yang, M. Sanju´an, W. Xiang, H. Zhu, Pitchfork bifurcation and vibrational resonance in a fractional-order duffing oscillator, *Pramana – J. Phys.* **81**, 943–957 (2013).

[16] B. Deng, J. Wang, X. Wei, H. Yu, H. Li, Theoretical analysis of vibrational resonance in a neuron model near a bifurcation point, *Phys. Rev. E* **89**, 062916 (2014).

[17] T. Mbong, S. S. Martin, C. Tchawoua, the effect of nonlinear damping on vibrational resonance and chaotic behavior of a beam fixed at its two ends and prestressed, *Commun. Nonlinear Sci.* **22**, 228 – 243 (2015).

[18] T. O. Roy-Layinde, J. A. Laoye, O. Popoola, U. Vincent, Analysis of vibrational resonance in bi-harmonically driven plasma, *Chaos* **26**(9)**,** 093117 (2016).

[19] T. O. Roy-Layinde, J. A. Laoye, O. O. Popoola, U. E. Vincent, P. V. E. McClintock, Vibrational resonance in an inhomogeneous medium with periodic dissipation, *Phys. Rev. E* **96,** 032209 (2017).

[20] J. H. Yang, H. Zhu, Vibrational resonance in duffing systems with fractional order damping, *Chaos* **22** (1), 013112 (2012).

[21] J. Yang, M. A. Sanjuan, H. Liu, Bifurcation and resonance in a fractional mathieu-duffing oscillator, *J. Sound Vibr.* **88,** 1–8 (2015).

[22] W. Guo, L. Ning, Vibrational resonance in a fractional order quintic oscillator system with time delay feedback, *Intern. J. Bifurc. Chaos* **30**(02), 2050025(1 – 18) (2020).

[23] C. Jeevarathinam, S. Rajasekar, M. A. F. Sanju´an, Theory and numerics of vibrational resonance in duffing oscillators with time-delayed feedback, *Phys. Rev. E* **83,** 066205 (2011).

[24] J. H. Yang, X. B. Liu, Controlling vibrational resonance in a multistable system by time delay, *Chaos* **20**(3), 033124 (2010).
[25] J. H. Yang, X. B. Liu, Controlling vibrational resonance in a delayed multistable system driven by an amplitude-modulated signal, *Phys. Scripta* **82**(2), 025006 (2010).
[26] Z. Chen, L. Ning, Impact of depth and location of the wells on vibrational resonance in a triple-well system, *Pramana – J. Phys.* **90,** 49 (2018).
[27] U. E. Vincent, T. O. Roy-Layinde, O. O. Popoola, P. O. Adesina, P. V. E. McClintock, Vibrational resonance in an oscillator with an asymmetrical deformable potential, *Phys. Rev. E* **98** 062203 (2018).
[28] J. Laoye, T. Roy-Layinde, A. Omoteso, O. Popoola, U. Vincent, Vibrational resonance in a higher order nonlinear damped oscillator with rough potential, *Pramana – J. Phys.* **94,** 1 (2020)
[29] O. I. Olusola, O. P. Shomotun, U. E. Vincent, P. V. E. McClintock, Quantum vibrational resonance in a dual-frequency driven Tietz-Hua quantum well, *Phys. Rev. E* **101,** 052216 (2020).
[30] P. Yi, G. C. Rutledge, Molecular simulation of crystal nucleation in n-octane melts, *The J. of Chem. Phys.* **131** (13), 134902 (2009).
[31] P. Yi, G. C. Rutledge, Molecular simulation of bundle-like crystal nucleation from n-eicosane melts, *The J. of Chem. Phys.* **135** (2), 024903 (2011).
[32] P. Yi, C. R. Locker, G. C. Rutledge, Molecular dynamics simulation of homogeneous crystal nucleation in polyethylene, *Macromolecules* **46** (11), 4723 – 4733, (2013).
[33] D. A. Nicholson, G. C. Rutledge, Molecular simulation of flow-enhanced nucleation in n-eicosane melts under steady shear and uniaxial extension, *The J. of Chem. Phys.* **145** (24), 244903. (2016).
[34] M. Anwar, R. S. Graham, Molecular dynamics simulations of crystal nucleation in entangled polymer melts under start-up shear conditions, *The J. of Chem. Phys.* **150** (8), 084905 (2019).
[35] A. Koyama, T. Yamamoto, K. Fukao, Y. Miyamoto, Molecular dynamics simulation of polymer crystallization from an oriented amorphous state, *Phys. Rev. E* **65** 050801 (2002).
[36] M. S. Lavine, N. Waheed, G. C. Rutledge, Molecular dynamics simulation of orientation and crystallization of polyethylene during uniaxial extension, *Polymer* **44** (5), 1771 – 1779 (2003).
[37] T. C. Ionescu, C. Baig, B. J. Edwards, D. J. Keffer, A. Habenschuss, Structure formation under steady-state isothermal planar elongational flow of n-eicosane: A comparison between simulation and experiment, *Phys Rev. Lett***. 96**, 037802 (2006).
[38] C. Baig, B. J. Edwards, Atomistic simulation of crystallization of a polyethylene melt in steady uniaxial extension, *J. Non-Newtonian Fluid Mech.* **165** (17), 992 – 1004 (2010).
[39] C. Baig, B. J. Edwards, Atomistic simulation of flow-induced crystallization at constant temperature, *Europhys. Lett.* **89** (3), 36003 (2010).
[40] I. I. Blekhman, Vibrational Mechanics, (World Scientific, Singapore, 2000).
[41] D. Su, M. Chiu, and C. Chen, Simple two-frequency laser, *Precis. Eng*. **18,** 161 (1996).
[42] A. Maksimov, On the subharmonic emission of gas bubbles under two-frequency excitation, *Ultrasonics* 35, 79-86 (1997).
[43] E. D. Kaplan, Understanding GPS: Principles and Applications, (Artech House, London, 1996) .
[44] A. Kumar and P.P. Patil, Free vibration and connecting bolt constraint-based FEA analysis of heavy vehicle medium duty transmission gearbox housing made from AISI 4130 alloy material, Mathematics Applied to Engineering, 133-146 (2017).